

Helicopter tail rotor instability

Problem presented by

Alan Irwin

Westland Helicopters

Problem statement

Data obtained by Westland Helicopters from a simulation of a teetered tail rotor shows instability at sufficiently high forward velocity of the aircraft, and also indicates a rotor natural frequency at nearly three times the rotor rotation frequency. The Study Group was asked to provide an explanation of these observations. Using a linear model for the teetering motion and the umbrella ‘flap’ mode of the tail rotor blades, the Study Group showed that parametric terms, containing the forward velocity, provide excitation at frequencies which are once and twice the blade rotation frequency. Taking the classical damped Mathieu equation as a ‘toy’ model of the system, and observing the near 3:2 ratio between the natural rotor frequency and the second excitation frequency, suggested that the observed instability arises as the forward velocity passes into the 3:2 resonance tongue of the stability map of the Mathieu equation. The current ‘snapshot’ eigenvalue method, in use at Westland Helicopters, does not capture this instability. The Study Group recommended instead that Floquet theory be applied to a time-dependent linearised model.

Report prepared by

Alan Champneys (University of Bristol)

Study Group contributors

Andre Aigner (University of Exeter)
Sasha Balanov (University of Lancaster)
Alan Champneys (University of Bristol)
Rich Eyres (University of Bristol)
Mike Friswell (University of Bristol)
Jens Gravesen (Technical University of Denmark)
Chris Halse (University of Bristol)
Poul Hjorth (Technical University of Denmark)
Natalia Janson (University of Lancaster)
David Lloyd (University of Bristol)
John Ockendon (University of Oxford)
Sasha Silchenko (University of Lancaster)
David Wagg (University of Bristol)
Charles Wang (University of Lancaster)
Dave Wood (University of Warwick)
Jenny Wright (University of Bath)
Xu Xu (University of Aberdeen)

1 Executive summary

- Data from Westlands from a modal simulation of a teetered tail rotor shows instability at sufficiently high forward velocity of the aircraft.
- A linearised analysis is sufficient to capture this instability, due to the small teeter angles.
- Detailed modelling and simulation has been undertaken of a two-degree-of-freedom model, for the teetering motion and the umbrella ‘flap’ mode of the blades. Forward velocity enters via parametric excitation terms with frequencies once and twice per revolution.
- A near 3:1 parametric resonance between the teeter natural frequency and the rotor speed would appear to be responsible for the instability. This can be explained by analysing the classical Mathieu equation for the teeter degree of freedom only where the resonance tongue in question is the 3:2 resonance.
- The current ‘snapshot’ eigenvalue method within Westlands software is bound to fail to capture this instability.
- Instead, Floquet theory should be used, applied to the time-dependent system matrices.

2 Problem Description

This report considers a form of tail rotor instabilities described to us by Westland Helicopters Ltd (henceforth referred to as just Westlands) [4, 5]. It is our understanding that the results of those simulations are symptomatic of an instability problem on a real helicopter. A tail rotor typically has a far simpler design than the main rotor on a helicopter, since its main function is merely to counteract the torque produced by the main rotor. It does not contribute to the forward velocity of the aircraft, and in normal flight conditions is driven so as to rotate at a constant angular velocity Ω .

The particular rotor in question consists of four blades fixed at right angles to each other, with two opposite blades allowed collectively to ‘teeter’ about a hinge that is in the plane of the rotor disk, at an angle of $\alpha = 45^\circ$ to the axis of the two blades. Teetering here refers to an allowed degree of freedom γ about this axis with very little frictional damping (although aerodynamic effects provide significant damping in flight). The purpose of teetering is to provide strong pitch-flap coupling, and also to allow the rotor to compensate for the asymmetry due to the different characteristics of retreating and advancing blades.

For simplicity in this report we ignore any aerodynamic coupling, so that the behaviour of the two pairs of blades may be considered in isolation. Thus we consider the dynamics of a single pair of blades only, connected through their common amount of teeter. Furthermore, we assume that all blades (main and tail) rotate at constant frequency Ω and that there is no aerodynamic coupling from the fuselage or main rotor, so that the only input to the system is forward velocity of the whole aircraft, V_a .

Data was provided to us by Alan Irwin [4] from Westlands, further clarification of which was made available during the Study Group [5]. The data contains the results of a modal simulation of all four blades of the tail rotor in question, including degrees of freedom (DOF) for the teeter and just a few flexural modes of each blade. Several salient features can be observed

- For sufficiently low airspeeds e.g. $V_a = 100$ knots, the response of the teetering DOF is small amplitude (2.5° peak to peak) periodic motion, with period $T = 1/\Omega$, where the rotor speed is $\Omega = 16\text{Hz}$. The tip of each blade has a permanent 0.5° deviation, with a lower-amplitude (0.2°) quasi-periodic flapping motion superimposed.
- At higher airspeeds, e.g. $V_a \geq 150$ knots, the teeter response is no longer periodic, but contains significant modulation, and also transient growth (to about 6° peak to peak after 20 seconds of simulation). The large amplitude motion appears from time traces to have lower-frequency (1–18Hz) and higher-frequency (44–48Hz) components. Also, the flapping motion is now significantly more excited, giving rise to a quasi-periodic signal that grows to 3° peak to peak over 20 cycles. This rate of growth is greater than for teetering DOF
- It is clear that the excited flapping motion is with the two opposite blades very nearly in phase (in the colour version of ref. [5] the time traces for opposite blades are almost overlaid). This suggests that the dominant flexural mode is the ‘umbrella’ mode where opposing blades deflect in synchrony (see Fig. 1).

- It is noticeable in the unstable simulation (and to a much lesser extent at 100 Knots) that the frequency spectrum has subsidiary peaks at 44Hz and 48Hz, the latter of which is three times the blade frequency 16Hz. The 44Hz we assume to be a natural frequency of one of the modes. The evidence points to this being the natural frequency of teetering, since the umbrella mode can be ruled out, since there is almost no power at this frequency in the collective tip displacement. The power spectral density of these two peaks appears to overlap slightly in the unstable simulation (150 Knots).

The motion for the lower forward speeds is regarded as the normal mode of operation. The motion for the higher speeds is undesirable as the transient growth would lead to vibration problems and possible material failure on a real aircraft. Within the simulation code it can lead to convergence failure.

The main aims of the problem as presented to the Study Group were firstly to explain this instability using mathematical modelling, but *more crucially* to find ways of predicting such instabilities using eigenvalue analysis. One approach used by Westlands within their modal analysis model is an “eigenvalue snapshot” analysis. Here the system linearisation is taken instantaneously at fixed time intervals around the rotor cycle. The eigenvalues for these matrices are then averaged over the cycle to get an impromptu indication of instability. This is used because straightforward Floquet theory cannot be applied to simulation trajectories that do not repeat every cycle.

An earlier attempt to arrive at a mathematical model for the teetering instability was made in the undergraduate project by Claire Fenwick [2]. The modelling follows along the lines indicated in ref. [4] (see also Appendix B below) including simple models for lift and drag, but full geometric nonlinearity. This leads to an unwieldy set of ordinary differential equations, which are also hard to implement due to square root nonlinearities, and embedded integrations along the blade lengths.

During the Study Group, several earlier studies of rotor instability were discovered in the published literature [1, 3, 8, 9, 10, 11, 12, 13, 14]. None of these references modelled precisely the same situation, nor did they contain a stability analysis technique of direct relevance. Several of the references stem from a simple 2 degree of freedom (2DOF) linear time-dependent model due to Chas Stammers [11] of the pitch and flap motion of a general helicopter rotor. Our modelling eventually uncovers a similar-looking system of equations (see eqn. 11 below).

In the rest of this report, we first present the mathematical modelling (Section 3), then simulation and analysis of this and related models (Section 4). Finally Section 5 gives recommendations for how to capture the analysed instability using eigenvalue analysis.

3 Mathematical modelling

Modal analysis supplied by Westland together with their model simulations, suggests that the most important flexural mode of each blade is the fundamental out-of-plane ‘flapping’ vibration mode. When considering the pair of blades as a single entity, such vibrations can be described as a combination of in-phase flexural mode of the pairs of

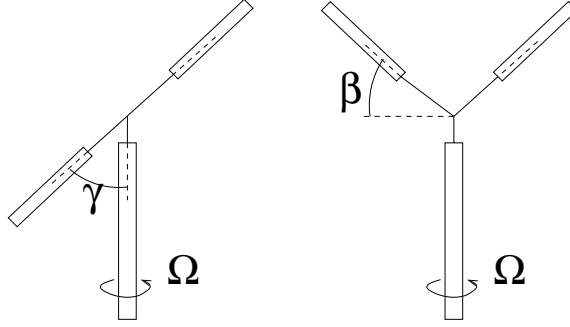


Figure 1: The teetering (γ) and umbrella (β) DOF, of the tail rotor that rotates at speed Ω . In this frame, forward air speed is a wind at speed V from left to right.

blades, which we call the **umbrella mode** and an out-of-phase asymmetric flexural mode. This latter mode has deflection largely in the same directions as the teetering DOF, and as already stated was not found to be significant in the simulation data. So we consider only the umbrella mode with modal displacement given by β (see Fig. 1).

A geometrically nonlinear model (using sines and cosines of γ and β) of these two degrees of freedom was derived in ref. [2], but is too unwieldy and certainly not of closed form. At the Study Group several attempts were made to linearise this model and to come up with a first principles linear model. The best attempt from the Study Group was a pair of equations of the form

$$\begin{bmatrix} 6.54 & 3.99 \\ 3.99 & 2.52 \end{bmatrix} \begin{bmatrix} \ddot{\gamma} \\ \ddot{\beta} \end{bmatrix} + \begin{bmatrix} d_1 \dot{\gamma} \\ d_2 \dot{\beta} \end{bmatrix} + \begin{bmatrix} 5 \times 10^5 + V_a^2 \sin^2(\Omega t - \alpha) & 4 \times 10^4 \\ 3 \times 10^4 + 170V_a \sin(\Omega t - \alpha) & 3 \times 10^4 \end{bmatrix} \begin{bmatrix} \gamma \\ \beta \end{bmatrix} = \begin{bmatrix} f_\gamma(t) \\ f_\beta(t) \end{bmatrix} \quad (1)$$

Where d_1 , d_2 are aerodynamic and structural damping terms, which can be set to zero for the worst case. Note the $V_a^2 \sin^2 \Omega t$ term. Simple trigonometry shows this to contain constant and $\sin 2\Omega t$ components. Note also that the constant 5×10^5 has been adjusted to make the teetering natural frequency equal to 44Hz ($\approx 3\Omega = 48 \text{ Hz}$). The functions $f_i(t)$ on the right represent the forcing terms of the two modes which are periodic, depending on the collective pitch.

Also at the Study Group, a strong argument was found to suggest that linearization is indeed valid. This argument, presented in Appendix A below, shows that, for a nonlinear model undergoing a limit cycle oscillation of small amplitude ε , replacement by a linear model with correct initial condition leads to an error of $O(\varepsilon^2)$.

Since the Study Group, several attempts have been made at a more rational modelling approach, most notably due to Jens Gravesen and Mike Friswell. The latter is presented in Appendix B below, which also relies on the rotation matrix notation introduced by Gravesen.

We present here a specific application of the modelling in Appendix B, using the following example parameter values taken from ref. [4]:

$$\begin{aligned} \alpha &= \frac{\pi}{4}, & \rho &= 1.225 \text{kg m}^{-3}, & c &= 0.32 \text{m}, \\ C_L &= 5.7, & C_D &= 0.01 & \Omega &= 101.47 \text{rad/s}. \end{aligned} \quad (2)$$

The constants involving integrals along the blade are estimated to be,

$$I_{10} = \int_0^{r_0} r dr = 1.7550\text{m}^2 \quad (3)$$

$$I_{11} = \int_0^{r_0} r w(r) dr = 1.2107\text{m}^3 \quad (4)$$

$$I_{12} = \int_0^{r_0} w(r) r^2 dr = 0.9042\text{m}^4 \quad (5)$$

$$I_{30} = \int_0^{r_0} r^3 dr = 3.9400\text{m}^4 \quad (6)$$

$$I_B = \int_0^{r_0} \sigma(r) r^2 dr = 13.08\text{kg m}^2 \quad (7)$$

$$m_b = 2 \times 2.524 = 5.048\text{kg m}^2 \quad (8)$$

$$m_t = 2I_B \sin^2 \alpha = 13.08\text{kg m}^2 \quad (9)$$

$$k_t = 1.905 \times 10^5 \text{N m} \quad (10)$$

and the natural frequency of the umbrella mode is 5.802Hz, although this is for a non-rotating blade.

The equations of motion then become

$$\begin{aligned} & \begin{bmatrix} 13.08 & 0 \\ 0 & 5.048 \end{bmatrix} \begin{Bmatrix} \ddot{\gamma} \\ \ddot{\beta} \end{Bmatrix} + \\ & \begin{bmatrix} 446.6 & -1.913V_a \sin(\Omega t - \alpha) \\ -1.913V_a \sin(\Omega t - \alpha) & 205.0 \end{bmatrix} \begin{Bmatrix} \dot{\gamma} \\ \dot{\beta} \end{Bmatrix} + \\ & \begin{bmatrix} 1.905 \times 10^5 + 0.9803V_a^2 \sin 2(\Omega t - \phi) & 0 \\ -194.1V_a \cos(\Omega t - \alpha) & 6708 \end{bmatrix} \begin{Bmatrix} \gamma \\ \beta \end{Bmatrix} = 0. \end{aligned} \quad (11)$$

These equations agree qualitatively with those derived by Gravesen, up to the appearance of a few extra terms and different parameter values. All three models (including the crude model (1) above) share the feature that the state-dependent aerodynamics in the $\ddot{\gamma}$ equation leads to a term

$$\propto k\gamma V_a^2 \sin 2(\Omega t + c)$$

for certain constants k and c . This is a parametric excitation term and will be crucial in what follows.

Note that the equations (11) were developed in Appendix B with the assumption of no reverse flow over the blade, which spans from 0.7m to 2m. From the Westlands data, the observed instability seems to occur for an air speed of approximately $V_a = 80\text{m/s}$. The inner part of the blade has a velocity of approximately $\Omega r = 70\text{m/s}$, showing that there will be reverse flow over part of the retreating blade. The effect of this reverse flow will be to change the numerical values in equation (11) and also include more parametric terms. Thus the numerical values from the linearised simulation, for example the air velocity for instability, are certainly not reliable. However, the important aspect is the demonstration that parametric terms are the only source of time-dependence in the model.

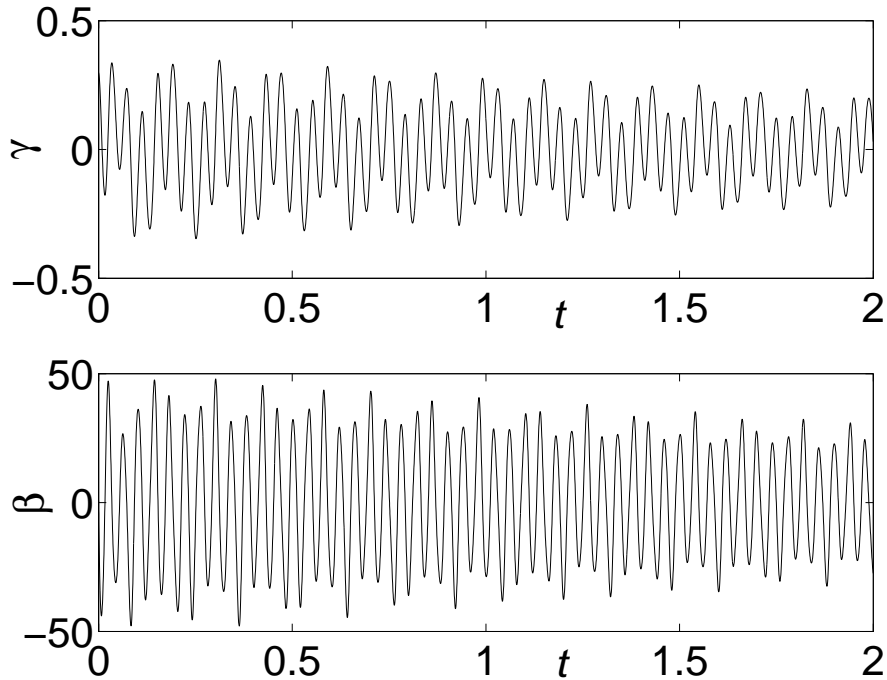


Figure 2: The stable response of eq. 11 for low airspeed $V_a < V_{\text{crit}}$

4 Parametric instability and simulation results

We first present the results of a simulation of the model (11). It was found that there is indeed a critical air velocity $V_a = V_{\text{crit}}$ below which stable, finite amplitude solutions are seen and beyond which solutions exhibit transient growth. Figure 3 shows the response for an air velocity just below the stability boundary $V_a < V_{\text{crit}}$ and figure 4 shows the unstable response for a small increase in air velocity. Note that for this model the stability boundary $V_a = V_{\text{crit}}$ is not 80m/s, but is significantly, perhaps as much as a factor of ten, higher. This may be due to some of the parameter uncertainties mentioned at the end of the previous Section, or due to some inconsistency in our modelling.

In mathematical modelling there is often the concept of the toy model. This is a model for which the parameter values may be incorrect, there may be the wrong number of variables, wrong boundary conditions etc., but the essential feature of the full model is captured. Toy models are easier to understand and analyse, and hopefully their solutions explain what is going on in the true model. In this case, the full model is only a simple 2DOF linear time-dependent set of ODEs, so it should not be much trouble to formally reduce the full model to a toy one, but for brevity's sake we do not do so here.

The toy model we introduce is as follows:

$$x'' + d_1 x' + (\kappa^2 + V^2(1 - \cos \tau))x = 0, \quad (12)$$

$$y'' + d_2 y' + k_2 y = f + cx. \quad (13)$$

Here x and y represent rescaled versions of γ and β respectively. Time has also been rescaled so that $\tau = 2\Omega t$, and $'$ represents $d/d\tau$. The dimensionless parameter κ

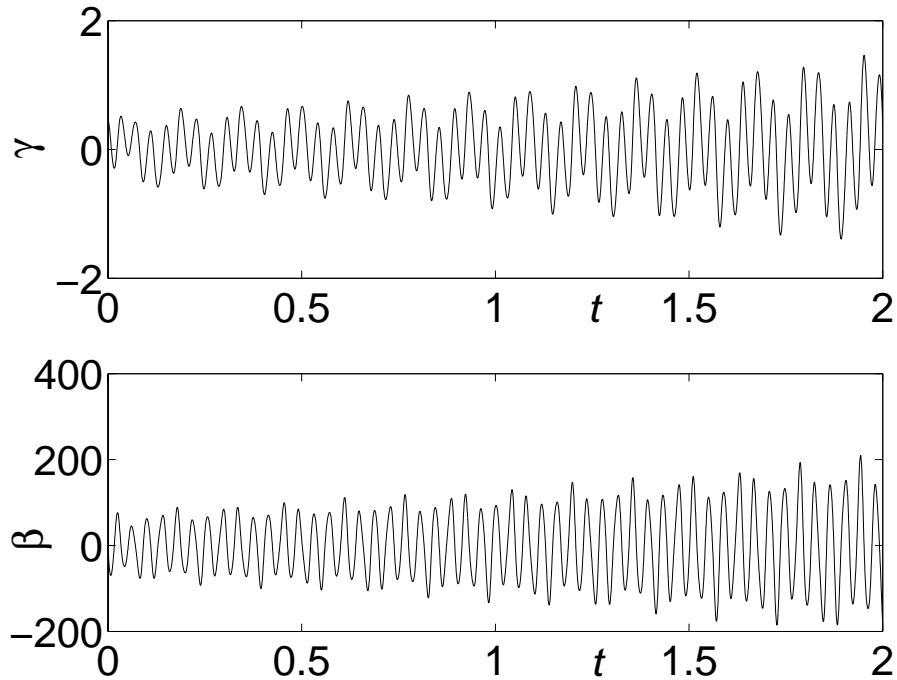


Figure 3: The unstable response of eq. (11) for high airspeed $V_a > V_{\text{crit}}$

represents the square of the ratio of the natural frequency of teetering to the excitation frequency 2Ω . The assumption that the natural frequency is a little bit less than 3Ω (44Hz vs. 48Hz) can be ensured by setting

$$\kappa^2 = \frac{9}{4} - \varepsilon$$

where ε is a small positive parameter representing the amount of the detuning.

Now, the x -equation (12) is just the classical damped Mathieu equation, which applies quite generally to parametrically excited one-degree-of-freedom systems; see for example ref. [6, 7]. The instability diagram for this model is well-known and is reproduced here in Fig. 4.¹ The arrow superimposed on that figure represents the effect of variation of the forward airspeed V_a . Note that for sufficiently large V_a , we move into the shaded region of instability. This is inside the ‘resonance tongue’ (dashed lines in Fig. 4) that without damping would correspond to a 3:2 resonance, That is, the free motion undergoing two oscillations every three cycles of the excitation frequency. Since the excitation frequency is 2Ω here, this motion would correspond to a response that is 3 times the rotor frequency.

Figs. 5 and 6 show simulation results for the toy model with parameter values chosen such that the damping is weaker in the flap degree of freedom y . The two sets of results represent $V < V_{\text{crit}}$ and $V > V_{\text{crit}}$ respectively. Note, in comparison to the graphs in ref. [5], that the results bear a striking qualitative resemblance to the modal simulation results at 150 knots, although the units in Fig. 4 are arbitrary so that one cannot draw direct quantitative comparison.

¹An asymptotic analysis of the equation is included in Appendix C.

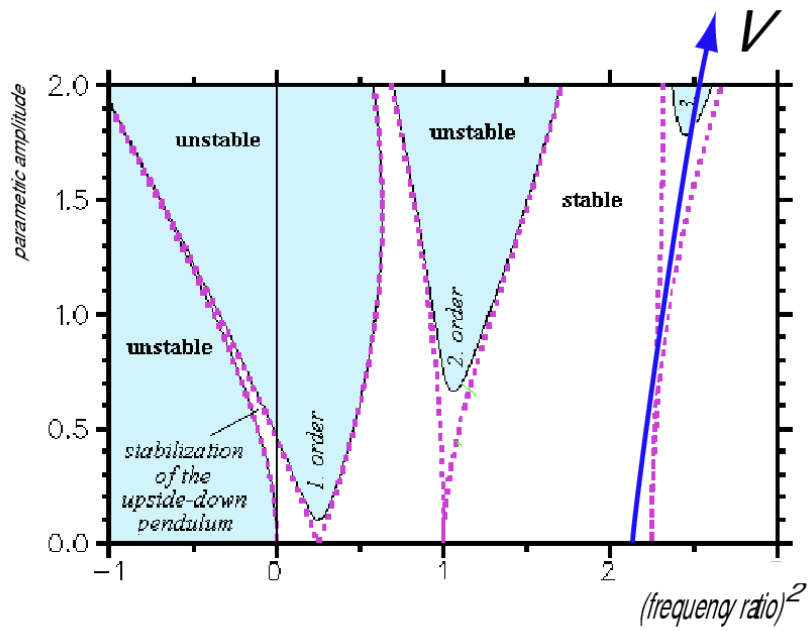


Figure 4: The stability analysis using the Mathieu equation. The superimposed arrow shows the effective path of the parameters under increase of forward speed (here marked as V).

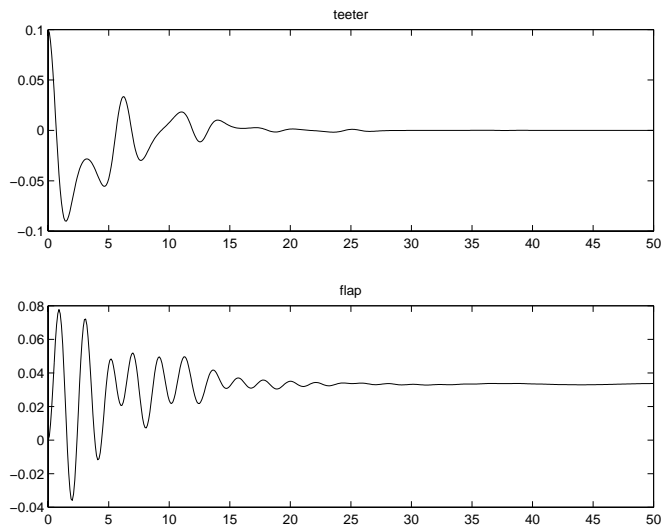


Figure 5: Stable solution of the simplified model (13) for $V < V_{\text{crit}}$

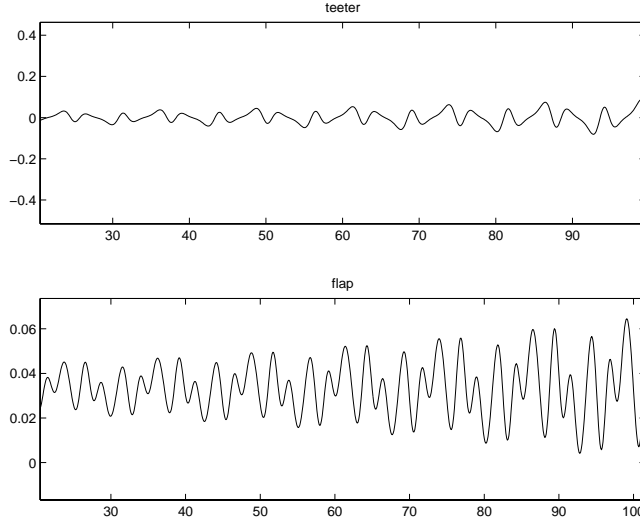


Figure 6: Unstable solution of the simplified model (13) for $V > V_{\text{crit}}$

The important aspect here has been to show that we can arrive at a rational explanation for what is observed by referring to parametric resonance in linearised equations of motion.

5 Predicting the instability in simulation software

The demonstration that the instability can be captured by a linear model with time-periodic coefficients is significant. This means that Floquet theory *can* be used to obtain a prediction/understanding of the instability in terms of matrices and eigenvalues, even if the response to the model is not periodic.

Floquet theory is described in several text books, for example ref. [6]. We show here how it applies to the kind of models that are dealt with in helicopter simulations. A general n -degree-of-freedom modal model, such as that used in Westland's simulation software could be written in the form

$$\mathbf{M}(t)\ddot{\mathbf{y}} + \mathbf{D}(t)\dot{\mathbf{y}} + \mathbf{K}(t)\mathbf{y} = \mathbf{f}(t). \quad (14)$$

Here \mathbf{M} , \mathbf{D} , \mathbf{K} are time-dependent $n \times n$; \mathbf{y} represents the n -dimensional vector of degrees of freedom, and $\mathbf{f}(t)$ are the state-independent forcing terms (note these are absent in the model (11)). Given steady aerodynamic conditions, we have that each of the time-dependent coefficients of the system matrices and forcing terms repeats every cycle. That is,

$$\mathbf{M}(t) = \mathbf{M}(t + T), \quad \mathbf{D}(t) = \mathbf{D}(t + T), \quad \mathbf{K}(t) = \mathbf{K}(t + T), \quad \mathbf{y}(t) = \mathbf{y}(t + T),$$

where the period $T = 1/\Omega$.

It is straightforward to write the 2nd-order n DOF system (14) as a $2n$ -dimensional first-order linear system

$$\dot{\mathbf{q}} = \mathbf{A}(t)\mathbf{q} + \mathbf{u}, \quad (15)$$

where \mathbf{q} is $2n$ -dimensional and $\mathbf{A}(t)$ is also periodic. To do this we write

$$\mathbf{q} = \begin{pmatrix} \mathbf{y} \\ \dot{\mathbf{y}} \end{pmatrix}, \quad \mathbf{A} = \begin{bmatrix} \mathbf{0} & \mathbf{I}_n \\ -\mathbf{M}^{-1}\mathbf{K} & -\mathbf{M}^{-1}\mathbf{D} \end{bmatrix}, \quad \mathbf{u} = \begin{pmatrix} \mathbf{0} \\ \mathbf{M}^{-1}\mathbf{f} \end{pmatrix}.$$

The stability of the fundamental solution is then obtained directly using Floquet theory. That is, we solve eq. (15) $2n$ times for solutions $\mathbf{y}^{(i)}(t)$ $i = 1 \dots 2n$, where the initial conditions are such that precisely the i th-component of $\mathbf{y}^{(i)}(0)$ is 1 and all other components zero. That is

$$\mathbf{y}_j^{(i)}(0) = \delta_{ij}$$

We solve over one period to find $\mathbf{v} = \mathbf{y}^{(i)}(T)$, and form $2n \times 2n$ so-called *Monodromy matrix*

$$\mathbf{M}_o = (\mathbf{v}_1 | \dots | \mathbf{v}_{2n})$$

composed of the vectors \mathbf{v} placed side by side.

Stability is determined precisely by the eigenvalues of \mathbf{M}_o , which are called the **Floquet multipliers** of the solution. The condition for stability is that all these eigenvalues lie inside the unit circle.

$$|\sigma(\mathbf{M}_o)| \leq 1$$

It is precisely by means of Floquet theory that the stability boundaries of the Mathieu equation, depicted in Fig. 4, are constructed. Those boundaries of even order correspond to Floquet multipliers = +1 (harmonic instability) and those with odd order to multipliers = -1 (subharmonic instability). Shaded regions thus correspond to where there exist Floquet multipliers greater than unity in modulus.

Finally let us see why a ‘snapshot’ eigenvalue approach, such as that adopted by Westlands, will not necessarily reproduce the results of Floquet analysis. To this end, we consider a simple parametrically excited system which is unstable and yet for which a snapshot analysis would predict stability. Consider the system

$$\ddot{x} + (1 + (1/2) \cos t)x + 2\varepsilon\dot{x} = 0, \quad \varepsilon > 0.$$

The Jacobian $\mathbf{A}(t)$ of the corresponding first order system is

$$\begin{bmatrix} 0 & 1 \\ -(1 + 1/2 \cos t) & -2\varepsilon \end{bmatrix}$$

which has eigenvalues $-\varepsilon \pm i\beta(t)$, for some periodic function β . For all times t , these eigenvalues lie in the left half-plane. That is, the snapshot method predicts *stable* solutions. But the pair of coefficients (amplitude,frequency ratio) = (1, 1/2) is in an *unstable region* of the Mathieu diagram (see Fig. 4), which remains unstable even in the presence of small damping ε .

In fact, for precisely the reasons underlying this simple example, snapshot eigenvalue analysis will almost always miss parametric resonance instabilities.

We are left with the following recommendation. **Westlands should replace their snapshot eigenvalue method by the correct application of Floquet theory to a time-dependent linearised model.** It may be that, in the course of the snapshot

analysis, the system matrix $\mathbf{A}(t)$ is being computed at discrete time instances around the rotor cycle. If this is the case, all that is required is to use this sequence of matrices (at the discrete time instances) to obtain a time discretisation of the linear system (15). Then Floquet theory can be applied to that system directly.

References

- [1] Boghiu D., Sinha S.C., Marghitu D.B., Stability and Control of a Parametrically Excited Rotating System, Part II: Controls, *Dynamics and control*, 8(1):19-35, 1998.
- [2] Fenwick C., *Mathematical Model of a Helicopter Tail Rotor*, Master of Engineering Project Thesis, University of Bristol, June 2002. *Supervisors: Prof. A.R. Champneys, Dr. M. Lowenberg.*
- [3] Friedmann P.P., Numerical Methods for Determining the Stability and Response of Periodic Systems with Applications to Helicopter Rotor Dynamics and Aeroelasticity, *Comp. and Maths. with Appls.*, 12A (1):131-148, 1986.
- [4] Irwin, A, Stability of Simple Teetering Tail Rotor, Private Communication (fax), 20 September 2001.
- [5] Irwin, A, Further Data from Simulation of Tail Rotor Private Communication (fax), 2 April 2003.
- [6] Jordan, D. W. and Smith, P., *Nonlinear Ordinary Differential Equations* (2nd Edition) OUP 1986.
- [7] Nayfeh, A.H. and Mook, D.T., *Nonlinear Oscillations*, Wiley 1979,
- [8] Krodkiewski J.M., Faragher J.S., Stabilization of Motion of Helicopter Rotor Blades using Delayed-Feedback Modelling, Computer Simulation and Experimental Verification, *Journal of Sound and Vibration*, 24(4):591-610, 2000.
- [9] Marghitu D.B., Sinha S.C., Boghiu D., Stability and Control of a Parametrically Excited Rotating System, Part I: Stability Analysis, *Dynamics and Control*, 8(1):5-18, 1998.
- [10] Pandiyan R., Sinha S.C., Periodic Flap Control of a Helicopter Blade in Forward Flight, *Journal of Vibration and Control*, 5:761-777, 1999.
- [11] Stammers C.W., The Flutter of a Helicopter Rotor Blade in Forward Flight, *The Aeronautical Quarterly*, February 1970.
- [12] Thornton B.S., A Bifurcation Method to Calculate Flutter Characteristics of a Helicopter Blade having Complex Damping, *Journal of the Franklin Institute*, 300(5,6):365-375, November-December 1975.
- [13] Tongue B.H., Flowers G., Nonlinear Rotorcraft Analysis, *Int. J. Non-Linear Mechanics*, 23 (3):189-203, 1988.

- [14] Article on *Rotor Failure over Wales*,
<http://news.bbc.co.uk/1/hi/wales/722180.stm>

A Justification of linearisation

The full model of the teetering tail rotor as analysed in [2] is nonlinear due to the sines and cosines of the teeter angle appearing many times via the various co-ordinate transformations. In nonlinear models, periodic responses are typically due to the presence of finite amplitude limit cycles. In linear models, periodic motion occurs whenever the linear operator has imaginary eigenvalues. Although sine and cosine nonlinearities are gross, we find that the response is limited to a few degrees. In this analysis, we determine the solution error introduced by linearising a single DOF toy model that contains a small-amplitude limit cycle oscillation.

Consider the following system of equations in polar co-ordinates.

$$\begin{aligned}\dot{r} &= r(\varepsilon - r) \\ \dot{\theta} &= 1\end{aligned}$$

It is trivial to see that it has a stable limit cycle at $r = \varepsilon$.

The linearisation for r is $\dot{r} = \varepsilon r$ with solution

$$r(t) = r_0 \exp \varepsilon t$$

In one cycle, starting at $r = \varepsilon$, a carefully asymptotic analysis shows that this will produce an error of $\varepsilon(1 - \exp 2\pi\varepsilon)$ compared to the full solution.

That is, the error is of order ε^2 . This is small if $\varepsilon < \frac{\ln 2}{2\pi} \approx 0.1$.

B Model Development – by Mike Friswell

The model has 2 DOF, namely the teeter angle, γ , and a DOF representing the participation of the *umbrella* flexible mode of the rotor, β . Other modes of the rotor could also be included, although experience with the detailed simulations has shown that this mode is involved in the teeter instability. The aim of the modelling is to obtain a linearized model by assuming that γ and β are small. This will enable a stability analysis to be performed. The development follows closely that of Irwin [4] and Fenwick [2].

B.1 Axes definitions

There are a number of axes that need to be defined. Consider the first axes set fixed in the rotor, with the rotor aligned along the x axis and bending in the z direction. Then the position of a point a distance r along the rotor in this axis set is,

$$\mathbf{r}_1 = \begin{Bmatrix} r \\ 0 \\ \beta w(r) \end{Bmatrix} \quad (16)$$

where $w(r)$ is the deflected shape of the umbrella mode. Note that r can be positive or negative, and the sign distinguishes between the two blades. To transform the displacement from this axis set to the stationary frame, we must,

- rotate by an angle α around the local z axis, since the teeter axis is not aligned with the rotor
- rotate by γ about the local x axis to allow for the teeter
- apply the constant rotational speed, $-\Omega$.

Thus, the position of the point on the rotor is

$$\mathbf{r} = \mathbf{R}_3(-\Omega t)\mathbf{R}_1(\gamma)\mathbf{R}_3(\alpha)\mathbf{r}_1 \quad (17)$$

where $\mathbf{R}_i(\theta)$ is the matrix describing a rotation of angle θ about the i 'th axis. For example,

$$\mathbf{R}_1(\theta) = \begin{bmatrix} 1 & 0 & 0 \\ 0 & \cos \theta & -\sin \theta \\ 0 & \sin \theta & \cos \theta \end{bmatrix}. \quad (18)$$

For the following analysis we need the derivatives of this position vector with respect to β , γ and time. This is a relatively straight-forward, if tedious, procedure, and only the results will be given here. Note also that these results have been linearized, so that higher order terms in β and γ have been neglected. Thus,

$$\frac{\partial \mathbf{r}}{\partial \beta} \approx w(r) \begin{bmatrix} -\gamma \sin(\Omega t) \\ -\gamma \cos(\Omega t) \\ 1 \end{bmatrix} \quad (19)$$

$$\frac{\partial \mathbf{r}}{\partial \gamma} \approx \begin{bmatrix} -[\gamma r \sin \alpha + \beta w(r)] \sin(\Omega t) \\ -[\gamma r \sin \alpha + \beta w(r)] \cos(\Omega t) \\ r \sin \alpha \end{bmatrix} \quad (20)$$

$$\dot{\mathbf{r}} = \frac{d\mathbf{r}}{dt} \approx \begin{bmatrix} -r\Omega \sin(\Omega t - \alpha) \\ -r\Omega \cos(\Omega t - \alpha) \\ r\dot{\gamma} \sin(\alpha) + \dot{\beta}w(r) \end{bmatrix} \quad (21)$$

$$\ddot{\mathbf{r}} = \frac{d^2\mathbf{r}}{dt^2} \approx \begin{bmatrix} -r\Omega^2 \cos(\Omega t - \alpha) \\ r\Omega^2 \sin(\Omega t - \alpha) \\ r\ddot{\gamma} \sin(\alpha) + \ddot{\beta}w(r) \end{bmatrix}. \quad (22)$$

B.2 Equations of motion

The equations of motion are obtained in the form,

$$\int_{-r_o}^{r_o} \sigma(r) \ddot{\mathbf{r}} \cdot \frac{\partial \mathbf{r}}{\partial \beta} dr = Q_\beta \quad (23)$$

$$\int_{-r_o}^{r_o} \sigma(r) \ddot{\mathbf{r}} \cdot \frac{\partial \mathbf{r}}{\partial \gamma} dr = Q_\gamma \quad (24)$$

where the integration is over the length of the two blades, r_o is the outer radius of the blade, $\sigma(r)$ is the mass per unit length, and the generalised forces are

$$Q_\beta = \int_{-r_o}^{r_o} \mathbf{F}(r) \cdot \frac{\partial \mathbf{r}}{\partial \beta} dr \quad (25)$$

$$Q_\gamma = \int_{-r_o}^{r_o} \mathbf{F}(r) \cdot \frac{\partial \mathbf{r}}{\partial \gamma} dr \quad (26)$$

and $\mathbf{F}(r)$ is the external force per unit length of blade, in this case the aerodynamic lift and drag forces.

From equations (19), (22) and (23)

$$\int_{-r_o}^{r_o} \sigma(r) \left[\gamma r w(r) \Omega^2 \sin \alpha + \ddot{\gamma} r w(r) \sin \alpha + \ddot{\beta} w(r)^2 \right] dr = Q_\beta \quad (27)$$

and from equations (20), (22) and (24)

$$\int_{-r_o}^{r_o} \sigma(r) \left[r \Omega^2 (\gamma r \sin \alpha - \beta w(r)) + \ddot{\gamma} r^2 \sin^2 \alpha + \ddot{\beta} r w(r) \sin \alpha \right] dr = Q_\gamma. \quad (28)$$

Combining equations of motion (27) and (28) gives,

$$\mathbf{M} \begin{Bmatrix} \ddot{\gamma} \\ \ddot{\beta} \end{Bmatrix} + \mathbf{K}_1 \begin{Bmatrix} \gamma \\ \beta \end{Bmatrix} = \begin{Bmatrix} Q_\gamma \\ Q_\beta \end{Bmatrix} \quad (29)$$

where,

$$\mathbf{M} = \int_{-r_o}^{r_o} \sigma(r) \begin{bmatrix} r^2 \sin^2 \alpha & r w(r) \sin \alpha \\ r w(r) \sin \alpha & w(r)^2 \end{bmatrix} dr \quad (30)$$

$$\mathbf{K}_I = \int_{-r_o}^{r_o} \sigma(r) \Omega^2 \begin{bmatrix} r^2 \sin \alpha & -r w(r) \\ r w(r) \sin \alpha & 0 \end{bmatrix} dr. \quad (31)$$

From the symmetry of the blades and the umbrella mode, $\sigma(r) = \sigma(-r)$ and $w(r) = w(-r)$, and thus

$$\mathbf{M} = 2 \int_0^{r_o} \sigma(r) \begin{bmatrix} r^2 \sin^2 \alpha & 0 \\ 0 & w(r)^2 \end{bmatrix} dr = \begin{bmatrix} m_t & 0 \\ 0 & m_b \end{bmatrix}, \quad (32)$$

$$\mathbf{K}_I = 2 \int_0^{r_o} \sigma(r) \Omega^2 \begin{bmatrix} r^2 \sin \alpha & 0 \\ 0 & 0 \end{bmatrix} dr = \begin{bmatrix} k_t & 0 \\ 0 & 0 \end{bmatrix}, \quad (33)$$

where equations (32) and (33) define m_t , m_b and k_t . Thus, the natural frequency in teeter, ignoring aerodynamic forces and any stiffness effect from the hinge, is $\omega_t = \sqrt{\frac{k_t}{m_t}} = \frac{\Omega}{\sin \alpha}$. Note that the blade stiffness has not yet been included. This will give a contribution to the stiffness matrix \mathbf{K}_1 such that

$$\mathbf{K}_I \rightarrow \mathbf{K}_I + \begin{bmatrix} 0 & 0 \\ 0 & k_b \end{bmatrix} \quad (34)$$

where k_b is the modal stiffness of the blade. Of course k_b should include the centrapedal stiffening due to the blade rotation.

B.3 The aerodynamic forces

It remains to calculate the aerodynamic forces. This requires the calculation of the relative air velocity in coordinates moving with the blade. The lift and drag forces are then calculated, and transformed to stationary coordinates. At each step second and higher order terms are neglected. The aerodynamic model is relatively simple in that the lift and drag forces, L and D , are

$$L = \frac{1}{2}\rho c V^2 C_L \bar{\alpha}, \quad (35)$$

$$D = \frac{1}{2}\rho c V^2 C_D, \quad (36)$$

where ρ is the air density, c is the blade chord, and C_L and C_D are lift and drag coefficients, which are assumed to be constant. The velocity V is the magnitude of the relative air velocity perpendicular to the blade axis, and the drag force is in the same direction as this velocity, while the lift force is perpendicular. The effective angle of attack, $\bar{\alpha}$, consists of two parts,

$$\bar{\alpha} = \phi + \theta \quad (37)$$

where ϕ is due to the relative velocity and θ due to the teetering. The angle of attack due to the teetering is given by

$$\sin \theta = \operatorname{sgn}(r) \sin \gamma \sin \alpha \quad (38)$$

or to first order,

$$\theta \approx \operatorname{sgn}(r) \gamma \sin \alpha \quad (39)$$

where sgn is the signum function. The use of the signum function is required because the angles of attack of the different blades have opposite signs.

The relative air velocity is computed by subtracting the blade velocity from the air velocity. In axes fixed in the blade, the blade velocity is, to first order,

$$\mathbf{V}_b = \mathbf{R}_3(-\alpha)\mathbf{R}_1(-\gamma)\mathbf{R}_3(\Omega t) \frac{d\mathbf{r}}{dt} \approx \begin{Bmatrix} 0 \\ -r\Omega \\ \gamma r\Omega \cos \alpha + \dot{\gamma}r \sin \alpha + \dot{\beta}w(r) \end{Bmatrix} \quad (40)$$

If the air velocity has magnitude V_a in the negative x direction in the stationary coordinate frame, then in axes fixed in the blade the air velocity is, to first order,

$$\mathbf{V}_a = -V_a \mathbf{R}_3(-\alpha)\mathbf{R}_1(-\gamma)\mathbf{R}_3(\Omega t) \mathbf{e}_1 \approx -V_a \begin{Bmatrix} \cos(\Omega t - \alpha) \\ \sin(\Omega t - \alpha) \\ -\gamma \sin(\Omega t) \end{Bmatrix} \quad (41)$$

Thus, the relative velocity \mathbf{V}_r is

$$\mathbf{V}_r = \mathbf{V}_a - \mathbf{V}_b \approx \begin{Bmatrix} -V_a \cos(\Omega t - \alpha) \\ r\Omega - V_a \sin(\Omega t - \alpha) \\ V_a \gamma \sin(\Omega t) - \gamma r\Omega \cos \alpha - \dot{\gamma}r \sin \alpha - \dot{\beta}w(r) \end{Bmatrix}. \quad (42)$$

The important terms are the velocities in the y and z direction which are perpendicular to the blade axes, and are zeroth and first order respectively. Thus ϕ is first order, $\tan \phi \approx \phi$,

$$V^2 \approx [r\Omega - V_a \sin(\Omega t - \alpha)]^2, \quad (43)$$

and

$$V^2 \phi \approx \text{sgn}(r) [r\Omega - V_a \sin(\Omega t - \alpha)] \times \left[V_a \gamma \sin(\Omega t) - \gamma r \Omega \cos \alpha - \dot{\gamma} r \sin \alpha - \dot{\beta} w(r) \right]. \quad (44)$$

The expression for $V^2 \phi$ assumes that $r\Omega > V_a$ and the signum function is required because of the different directions of the velocity of the two blades.

Since $\bar{\alpha}$ and ϕ are both first order, the lift force in axes fixed in the blade is,

$$\mathbf{L}_b \approx \frac{1}{2} \rho c V^2 C_L \bar{\alpha} \begin{Bmatrix} 0 \\ -\phi \\ 1 \end{Bmatrix} \approx \frac{1}{2} \rho c V^2 C_L \bar{\alpha} \mathbf{e}_3. \quad (45)$$

Thus the lift force in the fixed co-ordinate frame is,

$$\begin{aligned} \mathbf{L} &\approx \frac{1}{2} \rho c V^2 C_L \bar{\alpha} \mathbf{R}_3(-\Omega t) \mathbf{R}_1(\gamma) \mathbf{R}_3(\alpha) \mathbf{e}_3 \\ &\approx \frac{1}{2} \rho c V^2 C_L \bar{\alpha} \begin{Bmatrix} 0 \\ 0 \\ 1 \end{Bmatrix}. \end{aligned} \quad (46)$$

Then, from equations (19) and (20),

$$\mathbf{L} \cdot \frac{\partial \mathbf{r}}{\partial \beta} \approx \frac{1}{2} \rho c V^2 C_L \bar{\alpha} w(r) \quad (47)$$

$$\mathbf{L} \cdot \frac{\partial \mathbf{r}}{\partial \gamma} \approx \frac{1}{2} \rho c V^2 C_L \bar{\alpha} r \sin \alpha. \quad (48)$$

Substituting these expressions into equations (25) and (26) and using the symmetry of blades and the responses, gives the linearised contribution of lift to the generalised forces as,

$$\begin{Bmatrix} Q_{L\gamma} \\ Q_{L\beta} \end{Bmatrix} \approx -\mathbf{C}_L \begin{Bmatrix} \dot{\gamma} \\ \dot{\beta} \end{Bmatrix} - \mathbf{K}_L \begin{Bmatrix} \gamma \\ \beta \end{Bmatrix} \quad (49)$$

where,

$$\mathbf{C}_L = \rho c C_L \begin{bmatrix} \Omega I_{30} \sin^2 \alpha & -V_a I_{11} \sin \alpha \sin(\Omega t - \alpha) \\ -V_a I_{11} \sin \alpha \sin(\Omega t - \alpha) & \Omega I_{12} \end{bmatrix} \quad (50)$$

$$\mathbf{K}_L = \rho c C_L \begin{bmatrix} k_{11} & 0 \\ k_{21} & 0 \end{bmatrix} \quad (51)$$

$$k_{11} = \Omega^2 I_{30} \sin \alpha (\cos \alpha - \sin \alpha) + \frac{1}{2} V_a^2 I_{10} \sin \alpha \times [(\cos \alpha - \sin \alpha) \{1 - \cos 2(\Omega t - \alpha)\} + \sin \alpha \sin 2(\Omega t - \alpha)] \quad (52)$$

$$k_{21} = \Omega V_a I_{11} [2(\sin \alpha - \cos \alpha) \sin(\Omega t - \alpha) - \sin \alpha \cos(\Omega t - \alpha)] \quad (53)$$

and

$$I_{jk} = \int_0^{r_0} r^j w(r)^k dr. \quad (54)$$

Note that if $\alpha = \frac{\pi}{4}$ then $\sin \alpha = \cos \alpha$ and equation (51) simplifies to

$$\mathbf{K}_L = \rho c C_L \begin{bmatrix} \frac{1}{2} V_a^2 I_{10} \sin^2 \alpha \sin 2(\Omega t - \alpha) & 0 \\ -\Omega V_a I_{11} \sin \alpha \cos(\Omega t - \alpha) & 0. \end{bmatrix} \quad (55)$$

The drag force, \mathbf{D}_b , in the blade coordinate system is

$$\mathbf{D}_b \approx \frac{1}{2} \rho c V^2 C_D \begin{pmatrix} 0 \\ 1 \\ \phi \end{pmatrix} \quad (56)$$

or transformed to the stationary axes, is

$$\begin{aligned} \mathbf{D} &\approx \frac{1}{2} \rho c V^2 C_D \mathbf{R}_3(-\Omega t) \mathbf{R}_1(\gamma) \mathbf{R}_3(\alpha) \begin{pmatrix} 0 \\ 1 \\ \phi \end{pmatrix} \\ &\approx \frac{1}{2} \rho c V^2 C_D \begin{pmatrix} \sin(\Omega t - \alpha) \\ \cos(\Omega t - \alpha) \\ \gamma \cos \alpha + \phi \end{pmatrix}. \end{aligned} \quad (57)$$

Using an identical procedure to that for the lift force,

$$\mathbf{D} \cdot \frac{\partial \mathbf{r}}{\partial \beta} \approx \frac{1}{2} \rho c V^2 C_D w(r) \phi \quad (58)$$

$$\mathbf{D} \cdot \frac{\partial \mathbf{r}}{\partial \gamma} \approx \frac{1}{2} \rho c V^2 C_D [\cos \alpha \{w(r) - r \sin \alpha\} \gamma - \cos \alpha w(r) \beta + w(r) \phi]. \quad (59)$$

Although these terms may be calculated as the linearised contribution to the generalised forces, it should be noted that in general $C_D \ll C_L$. In the example $C_D = 0.01$ and $C_L = 5.7$. Thus C_D is a first order order term, and therefore the contribution of the drag to the generalised force is second order and will be ignored.

C Asymptotic analysis of the damped Mathieu Equation

The following well-known example illustrates the effect of damping on parametric resonance.

Suppose that, instead of the full blade model, we consider

$$\ddot{\beta} + \mu \varepsilon \dot{\beta} + (1 + \nu \varepsilon + \lambda \varepsilon \cos 2t) \beta = 0, \quad (60)$$

where $\dot{\cdot}$ denotes the t -derivative, and the second term models the damping. (Notation in this appendix will be not be the same as in the main text, but β and t are analogous to x and Ωt in equation (12). We think of ε as a small parameter, $\mu \geq 0$ measures

the damping, $\lambda \geq 0$ measures the excitation amplitude, and ν can have either sign and measures the detuning.) A multiscale asymptotic expansion with

$$\beta \sim \beta_0(t, \tau) + \varepsilon \beta_1(t, \tau) + \dots, \quad (61)$$

and $\tau = \varepsilon t$, gives that

$$\beta_0 = A(\tau) \cos t + B(\tau) \sin t. \quad (62)$$

To avoid secular terms in β_1 , we need

$$-2A' - \mu A - \lambda B/2 + \nu B = 0, \quad (63)$$

$$2B' + \mu B + \lambda A/2 + \nu A = 0, \quad (64)$$

where $'$ denotes the τ -derivative. Hence

$$4A'' + 4\mu A' + (\mu^2 + \nu^2 - \lambda^2/4)A = 0. \quad (65)$$

So for the undamped equation ($\mu = 0$, the classical Mathieu equation) there is instability for $\lambda/2 > |\nu|$. But for the damped equation ($\mu > 0$) the region of instability is $\lambda/2 > \sqrt{\nu^2 + \mu^2}$. This gives an analytic way of understanding the lower boundary of the unstable regions in Figure 4.